Infrared absorption of CH3OSO and CD3OSO radicals produced upon photolysis of CH3OS(O)Cl and CD3OS(O)Cl in p-H2 matrices

Yu-Fang Lee, Lin-Jun Kong, and Yuan-Pern Lee

Citation: The Journal of Chemical Physics **136**, 124510 (2012); doi: 10.1063/1.3696894
View online: http://dx.doi.org/10.1063/1.3696894
View Table of Contents: http://scitation.aip.org/content/aip/journal/jcp/136/12?ver=pdfcov
Published by the AIP Publishing

Infrared absorption of CH_3OSO and CD_3OSO radicals produced upon photolysis of $CH_3OS(O)Cl$ and $CD_3OS(O)Cl$ in *p*-H_2 matrices

Yu-Fang Lee,[1] Lin-Jun Kong,[1] and Yuan-Pern Lee[1,2,a)]
[1]*Department of Applied Chemistry and Institute of Molecular Science, National Chiao Tung University, 1001 Ta-Hsueh Rd., Hsinchu 30010, Taiwan*
[2]*Institute of Atomic and Molecular Sciences, Academia Sinica, Taipei 10617, Taiwan*

(Received 18 January 2012; accepted 2 March 2012; published online 29 March 2012)

Irradiation at 239 ± 20 nm of a *p*-H_2 matrix containing methoxysulfinyl chloride, $CH_3OS(O)Cl$, at 3.2 K with filtered light from a medium-pressure mercury lamp produced infrared (IR) absorption lines at 3028.4 (attributable to ν_1, CH_2 antisymmetric stretching), 2999.5 (ν_2, CH_3 antisymmetric stretching), 2950.4 (ν_3, CH_3 symmetric stretching), 1465.2 (ν_4, CH_2 scissoring), 1452.0 (ν_5, CH_3 deformation), 1417.8 (ν_6, CH_3 umbrella), 1165.2 (ν_7, CH_3 wagging), 1152.1 (ν_8, S=O stretching mixed with CH_3 rocking), 1147.8 (ν_9, S=O stretching mixed with CH_3 wagging), 989.7 (ν_{10}, C−O stretching), and 714.5 cm^{-1} (ν_{11}, S−O stretching) modes of *syn*-CH_3OSO. When $CD_3OS(O)Cl$ in a *p*-H_2 matrix was used, lines at 2275.9 (ν_1), 2251.9 (ν_2), 2083.3 (ν_3), 1070.3 (ν_4), 1056.0 (ν_5), 1085.5 (ν_6), 1159.7 (ν_7), 920.1 (ν_8), 889.0 (ν_9), 976.9 (ν_{10}), and 688.9 (ν_{11}) cm^{-1} appeared and are assigned to *syn*-CD_3OSO; the mode numbers correspond to those used for *syn*-CH_3OSO. The assignments are based on the photolytic behavior and a comparison of observed vibrational wavenumbers, infrared intensities, and deuterium isotopic shifts with those predicted with the B3P86/aug-cc-pVTZ method. Our results extend the previously reported four transient IR absorption bands of gaseous *syn*-CH_3OSO near 2991, 2956, 1152, and 994 cm^{-1} to 11 lines, including those associated with C−O, O−S, and S=O stretching modes. Vibrational wavenumbers of *syn*-CD_3OSO are new. These results demonstrate the advantage of a diminished cage effect of solid *p*-H_2 such that the Cl atom, produced via UV photodissociation of $CH_3OS(O)Cl$ *in situ*, might escape from the original cage to yield isolated CH_3OSO radicals. © *2012 American Institute of Physics*. [http://dx.doi.org/10.1063/1.3696894]

I. INTRODUCTION

The oxidation of reduced sulfur compounds such as dimethyl sulfide (DMS, CH_3SCH_3),[1] dimethyl disulfide (DMDS, CH_3SSCH_3), and methanethiol (or methyl mercaptan, CH_3SH), plays an important role in the formation of acid rain and cloud in the atmosphere.[2] CH_3SO_2, existing in three isomeric forms: methylsulfonyl (CH_3SO_2), methylthio peroxyl (CH_3SOO), and methoxy sulfinyl (CH_3OSO), has been proposed to be an important intermediate in the oxidation of reduced sulfur compounds in the atmosphere.[3–5] Although theoretical computations predict that CH_3OSO is the most stable among these three isomers, present reports indicate that it is less likely to be produced via direct reactions involving CH_3S with O_2 because of a large barrier; photoisomerization from CH_3SO_2 or CH_3SOO might, however, lead to the formation of CH_3OSO.[6–12] CH_3OSO might also play an important role in the combustion of fuels containing sulfur species at high temperature, similar to the key role that HOSO plays in the combustion of sulfur-rich fossil fuels.[13]

According to quantum-chemical computations, two conformers of CH_3OSO are stable, with *syn*-CH_3OSO more stable than *anti*-CH_3OSO by ~8 kJ mol^{-1}. The barrier for conversion from *anti*-CH_3OSO to *syn*-CH_3OSO is only 1−3 kJ mol^{-1}. In comparison with other isomers, *syn*-CH_3OSO is more stable than CH_3SO_2 by 9−56 kJ mol^{-1} (Refs. 6, 7, 10, 11, 12, and 14) and CH_3SOO by 236−314 kJ mol^{-1}.[8,9,12] The barrier for isomerization of CH_3SO_2 to CH_3OSO is reported to be 98 kJ mol^{-1} (Ref. 6) or 166−199 kJ mol^{-1}.[9,11,12] Reactions of CH_3 with SO_2 might proceed via two paths: a nearly barrierless channel to produce CH_3SO_2 and another channel with a barrier 47−58 kJ mol^{-1} to produce *anti*-CH_3OSO and *syn*-CH_3OSO.[6] The reaction of CH_3S with O_2 is expected to yield mainly CH_3SOO, which might subsequently produce CH_3SO and other secondary products.[14]

Gaseous CH_3OSO was produced with collisional electron transfer and detected with a neutralization-reionization mass spectrometer by Frank and Turecek.[6] The electron-paramagnetic-resonance spectrum of CH_3OSO in the condensed phase was also reported.[15,16] Our laboratory has employed a step-scan Fourier-transform infrared (FTIR) spectrometer to detect four transient infrared (IR) absorption bands of gaseous *syn*-CH_3OSO, produced upon irradiation at 248 nm of $CH_3OS(O)Cl$ in excess N_2 or CO_2.[17] The intense band near 1152 cm^{-1} was attributed to two overlapping bands at 1154 ± 3 and 1151 ± 3 cm^{-1}, assigned to the S=O stretching mixed with CH_3 rocking (ν_8) and the S=O stretching mixed with CH_3 wagging (ν_9) modes, respectively. A second feature at 994 ± 6 cm^{-1}, with only half of the band observed because of a limitation in the spectral range of the detector,

a)Author to whom correspondence should be addressed. Electronic mail: yplee@mail.nctu.edu.tw. FAX: 886-3-5713491.

was assigned to the C−O stretching (ν_{10}) mode. Two weak bands at 2991 ± 6 and 2956 ± 3 cm^{-1} were assigned to the CH_3 antisymmetric stretching (ν_2) and symmetric stretching (ν_3) modes, respectively, but the important O−S stretching mode was unobserved because of the limited spectral range of the photovoltaic detector.

The matrix-isolation technique is suitable for further spectral investigation of CH_3OSO because the sample can be accumulated over an extended period to increase its absorbance so that weaker lines might be observed. Furthermore, because of the small widths of lines and the absence of rotation in matrices because of the low temperature, overlapped bands such as ν_8 and ν_9 in gaseous *syn*-CH_3OSO might be resolved in the matrix.[18,19] The small amount of samples required for matrix-isolation spectroscopy also makes isotopic experiments feasible. For conventional inert-gas matrices, however, the matrix cage effects typically prevent formation of free radicals from the photolysis of chloro compounds *in situ* because the Cl atom cannot escape from the original cage.[20] The diminished cage effect of the quantum solid *p*-H_2 as a matrix host has been demonstrated to allow the production of free radicals via photofragmentation[21–24] or bimolecular reactions[25–29] upon UV irradiation. For example, in our laboratory, irradiation with a mercury lamp at 254 nm of a *p*-H_2 matrix containing CH_3I and SO_2 at 3.2 K followed by annealing of the matrix produced prominent features at 633.8, 917.5, 1071.1, 1272.5, and 1416.0 cm^{-1} that are attributable to ν_{11} (C−S stretching), ν_{10} (CH_3 wagging), ν_8 (SO_2 symmetric stretching), ν_7 (SO_2 antisymmetric stretching), and ν_4 (CH_2 scissoring) modes of CH_3SO_2, respectively.[27] These results demonstrate that the cage effect of solid *p*-H_2 is diminished so that CH_3 radicals, produced via UV photodissociation of CH_3I *in situ*, might react with SO_2 to form CH_3SO_2 during irradiation and upon annealing. The present work on CH_3SO_2 isolated in a *p*-H_2 matrix extends the previous observation of two transient IR absorption bands of gaseous CH_3SO_2 at 1280 and 1076 cm^{-1} (Ref. 30) to five lines to include the important one associated with the C−S stretching mode.

We have extended the project to matrix-isolated CH_3OSO and CD_3OSO produced via UV photolysis of a *p*-H_2 matrix containing $CH_3OS(O)Cl$ and $CD_3OS(O)Cl$, respectively. Eleven fundamental vibrational modes of *syn*-CH_3OSO, including the C−O, O−S, and S=O stretching modes are characterized.

II. EXPERIMENTS AND COMPUTATIONS

The matrix sample substrate is a gold-plated copper block, cooled to 3.2 K with a closed-cycle refrigerator system (Janis RDK-415); it also serves as a mirror to reflect the incident IR beam to the detector.[25,31] Typically, a gaseous mixture of $CH_3OS(O)Cl$/*p*-H_2 (1/300−1/2000, flow rate 14.7−16.1 mmol h^{-1}) was deposited over a period of 2−6.5 h. IR absorption spectra were recorded with a FTIR spectrometer (Bomem, DA8) equipped with a KBr beam splitter and a HgCdTe detector at 77 K to cover the spectral range 450−4100 cm^{-1}. The IR spectrum of the sample at 3.2 K were recorded generally at resolution 0.25 cm^{-1} and averaged with 600 interferometric scans after each stage of the experiment. The IR beam was passed through a filter (2.40ILP-50, Andover Corp.) to block light with wavenumber greater than 4100 cm^{-1} to avoid reaction of Cl with vibrationally excited H_2 produced after absorption of the IR light.[32]

A medium-pressure mercury (Hg) lamp (200 W, China Electric, Model H200X) coupled with an interference filter passing either 239 ± 20 nm or 254 ± 10 nm serves as a source for initial photolysis. Transmission for Hg emission lines near 253.7 and 226.2 nm is ∼6.5% and 10.5%, respectively, for the 239 nm filter and ∼15% and 0%, respectively, for the 254 nm filter.

Normal H_2 (99.9999%, Scott Specialty Gases), after passing through a trap at 77 K, entered a copper cell filled with hydrous iron(III) oxide catalyst (Aldrich) and cooled with a closed-cycle refrigerator (Advanced Research Systems, DE204AF) for *p*-H_2 conversion. The efficiency of conversion was controlled by the temperature of the catalyst; the conversion temperature is typically set at 13 K at which the concentration of *o*-H_2 is less than 40 ppm.

$CH_3OS(O)Cl$ was synthesized[33] on slow addition of CH_3OH (∼1 g) to equal moles of Cl_2SO under stirring, followed by further addition of CH_3OH (0.4 g) and stirring for 30 min until no bubble was observed. The products were stored in a refrigerator at 253 K for a few days for completion of the reaction before being pumped under vacuum at 193 K to remove HCl and SO_2. For the synthesis of $CD_3OS(O)Cl$, CH_3OH was replaced with CD_3OH. CH_3OH (Absolute Grade, 100.0%, J. T. Baker), CD_3OH (isotopic purity 99.5%, Cambridge Isotope Laboratories), and Cl_2SO (>98%, Riedel–de Haën) were used without further purification.

The geometry and vibrational wavenumbers of CH_3OSO are well characterized.[17,30] In this work, we employed the GAUSSIAN 09 program to calculate the harmonic and anharmonic vibrational wavenumbers, and IR intensities of CH_3OSO and CD_3OSO with the B3P86 density-functional theory.[34] Dunning's correlation-consistent polarized-valence triple-zeta basis set, augmented with s, p, d, and f functions (aug-cc-pVTZ),[35,36] was employed. Harmonic vibrational wavenumbers were calculated analytically at each stationary point. The anharmonic effects were calculated with a second-order perturbation approach using effective finite-difference evaluation of the third and semidiagonal fourth derivatives.

III. EXPERIMENTAL RESULTS

A. Photolysis of $CH_3OS(O)Cl$/*p*-H_2 matrices

The IR spectrum of a sample of $CH_3OS(O)Cl$/*p*-H_2 (1/500) at 3.2 K is shown in Fig. 1(a) for some selected spectral regions. Lines at 3043.1, 3020.8, 2987.4, 2978.1, 2962.9, 1464.2, 1453.4, 1426.4, 1234.8, 1223.1, 1166.0, 965.2, 733.7, and 560.1 cm^{-1} are due to $CH_3OS(O)Cl$; those shown in Fig. 1(a) are marked as *. Our experimental observations are consistent with the anharmonic vibrational wavenumbers predicted for *syn*-$CH_3OS(O)Cl$, with four intense IR bands at 1231, 970, 709, and 453 cm^{-1} and some weaker

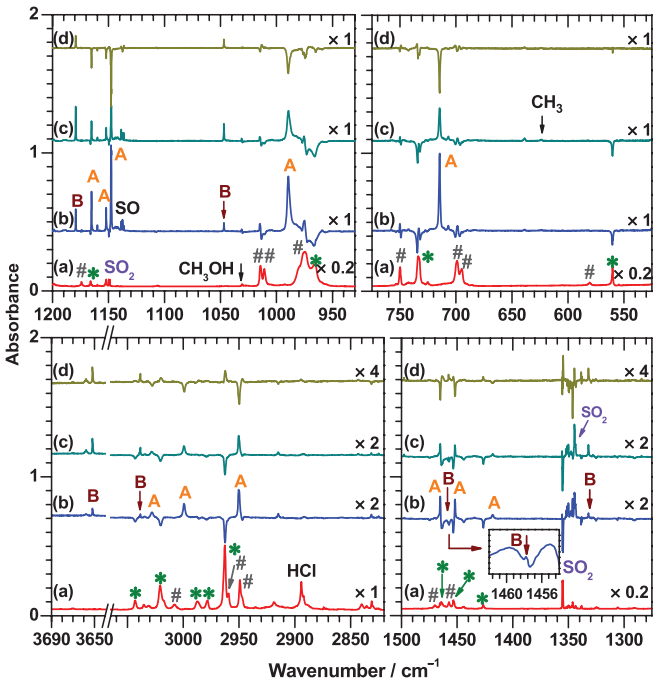

FIG. 1. (a) Partial IR spectra of a $CH_3OS(O)Cl/p\text{-}H_2$ (1/500) matrix after deposition for 3 h (trace a). Lines of $CH_3OS(O)Cl$ are marked as * and those of $(CH_3O)_2SO$ impurity are marked as #. (b) Difference spectra of the matrix in (a) after irradiation at 3.2 K and 239 ± 20 nm for 1.5 h. (c) Difference spectra obtained on further irradiation at 3.2 K and 239 ± 20 nm for an additional 1.5 h. (d) Difference spectra obtained on subtracting trace (b) from trace (c). Lines in groups A and B are assigned to *syn*-CH_3OSO and CH_2OH, respectively.

ones at 3036, 3014, 3001, 1472, 1438, 1434, 1144, and 547 cm^{-1}. The observations fit less satisfactorily with anharmonic vibrational wavenumbers predicted for *anti*-$CH_3OS(O)Cl$ with five intense IR bands at 1264, 994, 729, 470, and 445 cm^{-1} and several weaker ones near 3017, 2994, 2984, 1469, 1453, 1441, and 1165 cm^{-1}. Because *syn*-$CH_3OS(O)Cl$ is predicted to be more stable than *anti*-$CH_3OS(O)Cl$ by ~8 kJ mol^{-1} and the observed wavenumbers agree with *syn*-$CH_3OS(O)Cl$ better than with *anti*-$CH_3OS(O)Cl$, these lines are assigned to the *syn* conformer. The major impurity from synthesis of $CH_3OS(O)Cl$ is $(CH_3O)_2SO$, which absorbs at 3007.5, 2959.4, 2949.3, 1470.2, 1457.3, 1210.7, 1174.1, 1014.2, 1010.8, 974.7, 750.0, 699.2, 694.8, and 580.4 cm^{-1}, as marked # in Fig. 1(a). These features are similar to lines at 3028.0, 3005.1, 2960.5, 2952.8, 1469.1, 1467.8, 1457.6, 1454.0, 1208.6, 1187.9, 1016.6, 980.1, 748.3, 696.9, and 578.2 cm^{-1} reported for the GT form of $(CH_3O)_2SO$ in an Ar matrix, but contributions from the GG form cannot be excluded; the latter lines were reported at 3028.0, 3014.5, 3005.1, 2960.5, 2955.1, 1464.5, 1455.7, 1451.3, 1233.2, 1185.4, 1009.7, 972.1, 733.2, 693.8, 688.5, and 578.2 cm^{-1}.[37] A line at 1030.7 cm^{-1} is due to CH_3OH.[31] Some weaker lines near 1355.8/1355.4 and 1149.7/1148.7 cm^{-1} are due to SO_2 impurity.[27] Lines at 2894.1 and 2892.2 cm^{-1} are due to HCl.[38] Extremely weak lines at 1246.2 and 497.5 cm^{-1} might be due to Cl_2SO, consistent with values 1251 and 492 cm^{-1} reported in the gas phase.[39]

We found that irradiation of the matrix sample with the medium-pressure Hg lamp produced more intense lines of the CH_3OSO product in the initial stage of photolysis when a 239 ± 20 nm filter was used than when a 254 ± 10 nm filter was used, presumably CH_3OSO was dissociated with the UV light near 254 nm more readily than near 226 nm. We describe here only experiments with a filter passing light in the region 239 ± 20 nm.

Among various experiments, the following procedure provided the best results for identification of the CH_3OSO product: (1) irradiation of the matrix with light near 239 ± 20 nm for 1.5 h, and (2) further irradiation for additional 1.5 h. The matrix was maintained at 3.2 K during the photolysis and the recording of spectra.

Upon irradiation of the $CH_3OS(O)Cl/p\text{-}H_2$ (1/500) matrix at 239 ± 20 nm for 1.5 h, lines due to $CH_3OS(O)Cl$ (marked * in Fig. 1(a)) and SO_2 decreased in intensity, as shown in Fig. 1(b); those of $(CH_3O)_2SO$ (marked # in Fig. 1(a)), and Cl_2SO also decreased slightly. Trace (b) is a difference spectrum recorded upon irradiation near 239 ± 20 nm for 1.5 h after deposition. The difference spectrum was obtained on subtracting the spectrum recorded in the preceding step from that recorded after this step; features pointing upward thus indicate production, whereas those pointing downward indicate destruction. Trace (c) is a difference spectrum obtained after irradiation near 239 ± 20 nm for an additional 1.5 h. Some features increased in intensity more in this step, whereas some increased less. To differentiate this behavior, we subtracted trace (b) from trace (c), as shown in trace (d). The features pointing upwards in traces (b) and (c) but downwards in trace (d) are associated with species that were produced more in the initial stage and less in the second stage; they are indicated as group A. The features pointing upward in traces (b), (c), and (d) are thus associated with species that were produced more in the second stage than in the first stage; they are indicated as group B.

Lines in group A at 3028.4, 2999.5, 2950.4, 1465.2, 1452.0, 1417.8, 1165.2, 1152.1, 1147.8, 989.7, and 714.5 cm^{-1} show similar relative intensities in separate stages of various experiments; the line at 1147.8 cm^{-1} is overlapped with another one at 1147.4 cm^{-1}. These lines are assigned to *syn*-CH_3OSO, to be discussed in Sec. IV A. Lines in group B at 3651.9, 3038.5, 1457.6, 1332.1, 1179.2, and 1047.0 cm^{-1} have small intensities except the one at 1179.2 cm^{-1}. These features are readily assigned to CH_2OH because they have vibrational wavenumbers similar to those reported for CH_2OH in an Ar matrix at 3650, 1459, 1334, 1183, and 1048 cm^{-1}, with the latter two being more intense than others.[40,41] We also observed a line at 943.8 cm^{-1} due to atomic Cl (Ref. 42) and a line of SO at 1136.2 cm^{-1}.[43]

After prolonged irradiation, weak lines of CH_3, CH_3SO_2, CH_4, $ClSO_2$, and ClSO appeared. CH_3 absorbed at 3170.6, 1402.7/1402.3/1401.7, and 624.0 cm^{-1}, consistent with the reports for CH_3 of absorption at 3171.6/3171.4 (ν_1), 1402.7/1402.4/1401.7 (ν_3), and 624.0 (ν_2).[22,24] CH_3SO_2 absorbs at 1273.6/1273.0/1272.5 cm^{-1}, similar to the values reported for CH_3SO_2 produced from the reaction of $CH_3 + SO_2$ in a $p\text{-}H_2$ matrix.[27] Lines of CH_4 were observed at 3025.9/3025.1 (ν_3) and 1308.3 (ν_4),[21] and lines

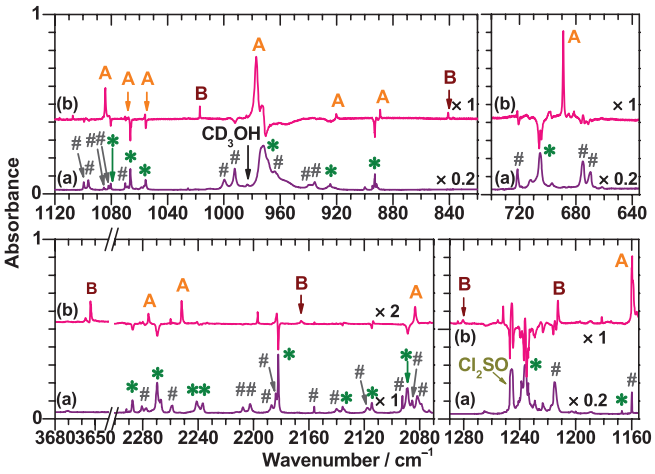

FIG. 2. (a) Partial IR spectra of a $CD_3OS(O)Cl/p\text{-}H_2$ (1/500) matrix after deposition for 4 h. Lines of $CD_3OS(O)Cl$ are marked as * and those of $(CD_3O)_2SO$ impurity are marked as #. (b) Difference spectra of the matrix in (a) after irradiation at 3.2 K and 239 ± 20 nm for 1 h. Lines in groups A and B are assigned to *syn*-CD_3OSO and CD_2OH, respectively.

at 1299.6/1298.7 and 1104.1/1103.1 cm^{-1} might be due to $ClSO_2$, consistent with the values 1311.0/1309.6 and 1099.8/1098.2 cm^{-1} reported for $ClSO_2$ in an Ar matrix.[44] ClSO was also observed at 1169.6 cm^{-1}, consistent with 1162.9 cm^{-1} reported in the gaseous phase.[45]

B. Photolysis of a $CD_3OS(O)Cl/p\text{-}H_2$ matrix

The IR spectrum of a sample of $CD_3OS(O)Cl/p\text{-}H_2$ (1/500) at 3.2 K is shown in Fig. 2(a). Lines at 2287.4, 2269.6, 2241.0, 2236.6, 2182.1, 2135.7, 2114.6, 2088.8, 1235.9, 1167.0, 1080.4, 1066.4, 1055.6, 971.8, 924.4, 892.7, 705.6, and 541.3 cm^{-1}, as marked * in Fig. 2(a), are due to $CD_3OS(O)Cl$, consistent with the anharmonic vibrational wavenumbers 2280, 2263, 2100, 1234, 1074, 1073, 1044, 967, 919, 887, 688, 530, and 451 cm^{-1} predicted with the B3P86/aug-cc-pVTZ method. Lines at 2280.6, 2277.3, 2258.5, 2207.7, 2202.5, 2187.0, 2183.9, 2156.3, 2140.1, 2117.9, 2092.6, 2085.5, 2081.9, 1215.1, 1159.9, 1099.5, 1096.3, 1085.2, 1082.0, 1070.1, 999.6, 992.3, 963.9, 940.0, 935.5, 721.4, 675.1, 669.8, and 559.9 cm^{-1}, as marked # in Fig. 2(a), are due to impurity $(CD_3O)_2SO$, consistent with the harmonic vibrational wavenumbers at 2349, 2337, 2329, 2304, 2188, 2174, 1247, 1120, 1103, 1081, 1080, 1069, 1065, 1013, 992, 947, 934, 908, 903, 700, 661, and 547 cm^{-1} predicted with the B3P86/aug-cc-pVTZ method. Line at 983.5 cm^{-1} is due to CD_3OH, consistent with value 988 cm^{-1} reported in the gas phase.[46] Lines at 1355.8/1355.4 and 1149.7/1148.7 cm^{-1} are due to SO_2 impurity. Lines at 1246.2 and 497.5 cm^{-1} are due to Cl_2SO.[39]

Trace (b) of Fig. 2 shows the difference spectrum of the $CD_3OS(O)Cl/p\text{-}H_2$ (1/500) matrix after irradiation at 239 ± 20 nm for 1 h. Lines due to $CD_3OS(O)Cl$ and SO_2 decreased in intensity, and lines in two groups appeared; those due to $(CD_3O)_2SO$ also decreased slightly. Lines in group A that were assigned to *syn*-CH_3OSO in the $CH_3OS(O)Cl/p\text{-}H_2$ experiments shifted to 2275.9, 2251.9, 2083.3, 1159.7, 1085.5, 1070.3, 1056.0, 976.9, 920.1, 889.0, and 688.9 cm^{-1}, as marked A in Fig. 2(a). Those in group B that were assigned to CH_2OH in the $CH_3OS(O)Cl/p\text{-}H_2$ shifted to 3653.6, 2165.9, 1280.5, 1212.9, 1017.1, and 840.7 cm^{-1}.

The ν_2 band of CH_3 observed at 624.0 cm^{-1} in Fig. 1(b) also shifted to 451.8 cm^{-1} for CD_3, similar to values 453 and 463 cm^{-1} observed in solid Ar and Ne, respectively.[47,48]

IV. DISCUSSION

Gaseous $CH_3OS(O)Cl$ at 300 K has an absorption cross section ~8 × 10^{-19} cm^2 molecule^{-1} near 248 nm.[17] The possible products after photolysis of $CH_3OS(O)Cl$ at 239 ± 20 nm are expected to be $CH_3OSO + Cl$, $CH_3 + ClSO_2$, and $CH_3O + ClSO$. According to Alligood *et al.*, only the S−Cl fission channel to produce Cl atom and CH_3OSO radical was observed upon photolysis of $CH_3OS(O)Cl$ at 248 nm.[49] Some vibrationally excited CH_3OSO radicals undergo subsequent dissociation to $CH_3 + SO_2$. The dissociation threshold to form $CH_3OSO + Cl$ is calculated to be 239 kJ mol^{-1}, corresponding to a wavelength of 501 nm.[49] With a filter to pass either 239 ± 20 nm or 254 ± 10 nm, we employed emission from a Hg lamp with the expectation that the light dissociates $CH_3OS(O)Cl$ and that the major products are CH_3OSO and Cl.

The photolysis of impurities $(CH_3O)_2SO$ and SO_2 must also be considered. The photolysis of $(CH_3O)_2SO$ at 248 nm was investigated by Alligood *et al.* who reported the main photodissociation products to be CH_3 and $CH_3OS(O)O$.[49] Although SO_2 has an absorption cross section ~2 × 10^{-19} cm^2 molecule^{-1} at 254 nm (Ref. 50) and ~3 × 10^{-19} cm^2 molecule^{-1} at 226 nm,[51] its dissociation threshold of 543 kJ mol^{-1} to form SO + O corresponds to a wavelength of ~220 nm.[52]

A. Assignments of lines in group A in the $CH_3OS(O)Cl/p\text{-}H_2$ experiments to *syn*-CH_3OSO

Considering that CH_3OSO is the expected product of photolysis and that the vibrational wavenumbers of five observed lines in group A near 2999.5, 2950.4, 1152.1, 1147.8, and 989.7 cm^{-1} are similar to the values of 2991 ± 6, 2956 ± 3, 1154 ± 3, 1151 ± 3, and 994 ± 6 cm^{-1} reported for gaseous *syn*-CH_3OSO,[17] we contend that lines in group A are likely due to *syn*-CH_3OSO.

As listed in Table I, quantum-chemical calculations using the B3P86/aug-cc-pVTZ method predict that the IR lines of *syn*-CH_3OSO with intensity greater than 10 km mol^{-1} have anharmonic vibrational wavenumbers near 2989 (ν_2), 2996 (ν_3), 1473 (ν_4), 1448 (ν_5), 1157 (ν_7), 1149 (ν_8), 1144 (ν_9), 995 (ν_{10}), and 698 (ν_{11}) cm^{-1}; some of the values are slightly modified from the previous report.[17] Our observed lines in group A at 3028.4, 2999.5, 2950.4, 1465.2, 1452.0, 1417.8, 1165.2, 1152.1, 1147.8, 989.7, and 714.5 cm^{-1} are within 2.3% of the predicted values. The relative IR intensities observed in these experiments are also consistent with the theoretical predictions except those associated with the ν_7−ν_9 modes, as compared in Table I. The deviations in

TABLE I. Comparison of harmonic and anharmonic vibrational wavenumbers (in cm^{-1}) and IR intensities (in km mol^{-1}, listed in parentheses) of *anti*-CH_3OSO and *syn*-CH_3OSO derived from experiments and calculations using the B3P86/aug-cc-pVTZ method.

		anti-CH_3OSO		*syn*-CH_3OSO			
ν_i	Mode[a]	Harmonic	Anharmonic	Harmonic	Anharmonic	Gas	*p*-H_2
ν_1	*a*-ν_{CH2}	3156 (5.0)	3016	3163 (4.5)	3019		3028.4 (7.7)[b]
ν_2	*a*-ν_{CH3}	3100 (23)	2962	3129 (15)	2989	2991 ± 6	2999.5 (18)
ν_3	*s*-ν_{CH3}	3031 (46)	2938	3046 (34)	2996	2956 ± 3	2950.4 (28)
ν_4	δ_s-CH2	1494 (16)	1478	1497 (12)	1473		1465.2 (10)
ν_5	*a*-δ_{CH3}	1486 (10)	1456	1479 (10)	1448		1452.0 (11)
ν_6	u_{CH3}	1460 (0.5)	1448	1455 (0.9)	1442		1417.8 (2.8)
ν_7	$\nu_{S=O}$	1195 (82)	1182	1181 (12)[c]	1157		1165.2 (18)
ν_8	ω_{CH3}	1185 (7.9)	1159	1166 (36)[c]	1149	1154 ± 3	1152.1 (11)
ν_9	ρ_{CH3}	1168 (0.7)	1147	1162 (33)[c]	1144	1151 ± 3	1147.8 (65)[d]
ν_{10}	ν_{C-O}	1046 (184)	1017	1028 (177)	995	994 ± 6	989.7 (177)
ν_{11}	ν_{S-O}	742 (132)	727	717 (103)	698		714.5 (101)
ν_{12}	$\delta_{OS=O}$	420 (2.2)	414	486 (5.5)	480		
ν_{13}	δ_{COS}/	241 (0.2)	245	254 (9.6)	264		
ν_{14}	τ_{C-O}	102 (1.7)	77	121 (2.9)	111		
ν_{15}	τ_{S-O}	46 (0.2)	33	75 (6.8)	50		
References		30	This work	30	This work	17	This work

[a]ν: stretch, δ: bend or deformation, δ_S: scissor, *u*: umbrella, ω: wag, ρ: rock, τ: torsion, *a*: antisymmetric, and *s*: symmetric.
[b]Integrated IR intensities relative to ν_{10} of *syn*-CH_3OSO are listed in parentheses.
[c]For *syn*-CH_3OSO, ν_7 is mainly ω_{CH3},ν_8 is $\nu_{S=O}/\rho_{CH3}$, and ν_9 is $\nu_{S=O}/\omega_{CH3}$.
[d]Overlapped with a line at 1147.4 cm^{-1}.

IR intensities of lines associated with the $\nu_7-\nu_9$ modes are likely due to a poor description of the mode mixing for these modes. For *anti*-CH_3OSO, the mode mixing is small and most intensity is with the ν_7 mode, whereas for *syn*-CH_3OSO, the three modes are mixed, with ν_7 approximately described as mainly CH_3 wagging, ν_8 as S=O stretching mixed with CH_3 rocking, and ν_9 as S=O stretching mixed with CH_3 wagging. All 11 modes predicted to have fundamental vibrational wavenumbers above 500 cm^{-1}, our detection limit, are observed in this work with relative intensities similar to predictions provides further support for the assignments of these lines in group A to *syn*-CH_3OSO. The assignments of two weak lines observed at 3028.4 and 1417.8 cm^{-1} should be considered as tentative because the two weak lines predicted at 3019 (ν_1) and 1442 (ν_6) cm^{-1} for *syn*-CH_3OSO has IR intensity less than 5 km mol^{-1}.

Syn-CH_3OSO and *anti*-CH_3OSO have similar vibrational wavenumbers, as listed in Table I. In our experiments, only one conformer appears to be observed because the observed lines show no splitting except the doublet at 1147.8 and 1147.4 cm^{-1}. If both conformers were present, the small differences in vibrational wavenumbers should result in several doublet lines for particular vibrational modes. Although we are unable to exclude positively the possibility of observed lines in group A being assigned to *anti*-CH_3OSO, we think that such an assignment is unlikely for the following reasons.

First, theoretical computations predict that *syn*-CH_3OSO is more stable than *anti*-CH_3OSO by ~8 kJ mol^{-1} (Refs. 6, 10, and 11); the *syn*-CH_3OSO should be dominant even at 300 K if we assume a Boltzmann distribution. The precursor $CH_3OS(O)Cl$ also has a *syn*-form. Second, the average deviation of observed wavenumbers from the predicted anharmonic vibrational wavenumbers for *syn*-CH_3OSO (0.8%) is slightly smaller than that from predictions for *anti*-CH_3OSO (1.1%). For the two most intense lines, the observed lines at 989.7 and 714.5 cm^{-1} are nearer those at 995 and 698 cm^{-1} predicted for *syn*-CH_3OSO than those at 1017 and 727 predicted for *anti*-CH_3OSO. Third, according to theoretical calculations, among ν_7 (S=O stretching), ν_8 (CH_3 wagging), and ν_9 (CH_3 rocking) modes of *anti*-CH_3OSO, only ν_7 has substantial IR intensity, whereas for *syn*-CH_3OSO all three modes are mixed and have comparable intensities. Our observations agree better with the latter.

The observed lines in group A do not match those reported for CH_3SO_2 in solid *p*-H_2 at 1416.0, 1272.5, 1071.1, 917.5, and 633.8 cm^{-1},[27] nor do they match those of $ClSO_2$ in solid Ar or those predicted for ClOSO.[44] Although two intense lines of $CH_3OS(O)O$, the product reported after photolysis of $(CH_3O)_2SO$ at 248 nm,[49] are predicted to have anharmonic vibrational wavenumbers (986 and 680 cm^{-1}) similar to those observed in group A (989.7 and 714.5 cm^{-1}), two additional intense lines predicted at 1261 and 1078 cm^{-1} were unobserved in our experiments.

B. Assignments of lines in group A in the $CD_3OS(O)Cl$/*p*-H_2 experiments to CD_3OSO

The deuterium-substitution experiment provides additional support for the assignment of lines in group A to *syn*-CH_3OSO. In Table II we compare the vibrational wavenumbers of lines in group A observed in the fully deuterated experiments with the harmonic and anharmonic vibrational wavenumbers of *syn*-CH_3OSO and *anti*-CH_3OSO computed quantum-chemically. To minimize the error of calculations, we also list the predicted values for *syn*-CH_3OSO in bracket in Table II. The predicted values are derived on multiplying

TABLE II. Comparison of harmonic (anharmonic) vibrational wavenumbers (in cm^{-1}) and IR intensities (in km mol^{-1}, listed in parentheses) of *anti*-CD_3OSO and *syn*-CD_3OSO derived from experiments and calculations using the B3P86/aug-cc-pVTZ method.

		anti-CD_3OSO		*syn*-CD_3OSO		
ν_I[a]	Mode[b]	Harmonic	Anharmonic	Harmonic	Anharmonic[c]	*p*-H_2
ν_1	a-ν_{CH3}	2340 (3.4)	2264	2348 (2.8)	2268 [2275]	2275.9 (5.0)[d]
ν_2	a-ν_{CH2}	2301 (15)	2224	2321 (10)	2243 [2251]	2251.9 (14)
ν_3	s-ν_{CH3}	2172 (33)	2074	2181 (24)	2117 [2085]	2083.3 (15)
ν_4	δ_s-CH2	1077 (6.6)	1082	1079 (4.1)	1077 [1071]	1070.3 (2.1)
ν_5	a-δ_{CH3}	1071 (4.1)	1060	1067 (6.4)	1053 [1056]	1056.0 (7.1)
ν_6	u_{CH3}	1117 (62)	1068	1103 (34)	1025 [1007]	1085.5 (25)
ν_7	$\nu_{S=O}$	1197 (75)	1183	1170 (70)	1158 [1166]	1159.7 (90)
ν_8	ω_{CH3}	947 (23)	935	934 (8.9)	917 [924]	920.1 (6.5)
ν_9	ρ_{CH3}	902 (2.1)	888	897 (2.6)	883 [886]	889.0 (3.2)
ν_{10}	ν_{CO}	1014 (145)	992	1008 (158)	982 [977]	976.9 (158)
ν_{11}	ν_{S-O}	708 (100)	695	691 (86)	676 [692]	688.9 (86)
ν_{12}	$\delta_{OS=O}$	407 (2.1)	401	467 (5.3)	462	
ν_{13}	δ_{COS}	223 (0.3)	226	236 (8.0)	244	
ν_{14}	τ_{C-O}	81 (1.0)	68	97 (5.5)	94	
ν_{15}	τ_{S-O}	40 (1.2)	36	63 (3.2)	51	

[a]We follow the order of vibrational modes assigned for *anti*-CH_3OSO.
[b]ν: stretch, δ: bend or deformation, δ_S: scissor, u: umbrella, ω: wag, ρ: rock, τ: torsion, a: antisymmetric, and s: symmetric.
[c]Predicted values listed in brackets are derived by multiplying observed wavenumbers of CH_3OSO with the calculated isotopic ratio, defined as the ratio of the anharmonic vibrational wavenumber of CD_3OSO to that of CH_3OSO predicted quantum chemically.
[d]Integrated IR intensities relative to ν_{10} of *syn*-CD_3OSO are listed in parentheses.

the observed wavenumber of CH_3OSO with the isotopic ratio, defined as the ratio of calculated anharmonic vibrational wavenumber of the D-substituted species to that of natural CH_3OSO. Most deviations between observed and predicted vibrational wavenumbers are within 4 cm^{-1} except for ν_7 and ν_6, which have deviations of 6 and 78 cm^{-1}, respectively. For the ν_7 mode, the deviation might be due to different extents of mixing in CH_3OSO and CD_3OSO. The wavenumbers of ν_5 and ν_6 are similar. We made the assignments of ν_5 and ν_6 according to the relative intensity of ν_5 and ν_6; the latter is predicted to be much greater than the former. The wavenumber order of ν_5 and ν_6 is the reverse of that of predicted anharmonic vibrational wavenumbers, but agrees with that of harmonic vibrational wavenumbers. For the ν_6 mode, the observed line at 1085.5 cm^{-1} agrees with the predicted harmonic vibrational wavenumber of 1103 cm^{-1}. It is unclear why the correction of anharmonicity for this mode reduces this value to 1025 cm^{-1}; the reduction is much larger than typical corrections.

According to theoretical predictions, the $\nu_7-\nu_9$ modes of *syn*-CH_3OSO are mixed, with comparable intensities, whereas those of *anti*-CH_3OSO are less mixed, with the ν_7 mode carrying the most intensity (Table I). In contrast, the ν_7 mode of *syn*-CD_3OSO is predicted to carry the most intensity, whereas the ν_8 mode of *anti*-CD_3OSO has more intensity than *syn*-CD_3OSO. Our observation of three lines at 1165.2, 1152.1, and 1147.8 cm^{-1} with comparable intensities for CH_3OSO and a prominent line at 1159.7 cm^{-1} for ν_7 and weak lines at 920.1 and 889.0 cm^{-1} for ν_8 and ν_9 modes of CD_3OSO strengthens the support for the assignments of lines in group A to *syn*-CH_3OSO/CD_3OSO.

In summary, we assigned lines in group A at 3028.4 cm^{-1} to ν_1 (CH_2 antisymmetric stretching), 2999.5 cm^{-1} to ν_2 (CH_3 antisymmetric stretching), 2950.4 cm^{-1} to ν_3 (CH_3 symmetric stretching), 1465.2 cm^{-1} to ν_4 (CH_2 scissoring), 1452.0 cm^{-1} to ν_5 (CH_3 deformation), 1417.8 cm^{-1} to ν_6 (CH_3 umbrella), 1165.2 cm^{-1} to ν_7 (CH_3 wagging), 1152.1 cm^{-1} to ν_8 (S=O stretching mixed with CH_3 rocking), 1147.8 cm^{-1} to ν_9 (S=O stretching mixed with CH_3 wagging), 989.7 cm^{-1} to ν_{10} (C−O stretching), and 714.5 cm^{-1} to ν_{11} (S−O stretching) modes of *syn*-CH_3OSO; the mode descriptions were made according to quantum-chemically predicted displacement vectors.

C. Assignments of lines in group B in the $CD_3OS(O)Cl/p$-H_2 experiments to CD_2OH

As described in Sec. III, in experiments with $CH_3OS(O)Cl/p$-H_2, lines in group B observed at 3651.9, 3038.5, 1457.6, 1332.1, 1179.2, and 1047.0 cm^{-1} agree well with those reported for CH_2OH in an Ar matrix at 3650, 1459, 1334, 1183, and 1048 cm^{-1}.[40,41] In experiments with $CD_3OS(O)Cl/p$-H_2, these lines shift to 3653.6, 2165.9, 1280.5, 1212.9, 1017.1, and 840.7 cm^{-1}. Although one would expect that CD_2OD would be the carrier, but the observed wavenumbers do not agree with the vibrational wavenumbers reported for CD_2OD in solid Ar at 2694, 1223, 1041, and 765 cm^{-1}.[41] Using the B3P86/aug-cc-pVDZ method, we computed anharmonic vibrational wavenumbers of CD_2OD to be 2715, 2400, 2203, 1013, 1029, 1234, and 756 cm^{-1} for $\nu_1-\nu_7$, consistent with the literature experimental values as listed in Table III.

As shown in Table III, the observed wavenumbers and relative IR intensities agree satisfactorily with the anharmonic vibrational wavenumbers and IR intensities predicted for CD_2OH with the B3P86/aug-cc-pVDZ method. To

TABLE III. Comparison of harmonic (anharmonic) vibrational wavenumbers (in cm^{-1}) and IR intensities (in km mol^{-1}, listed in parentheses) of CH_2OH, CD_2OD, and CD_2OH derived from experiments and calculations using the B3P86/aug-cc-pVTZ method.

		CH_2OH				CD_2OD			CD_2OH			
		Calculations		Experiment		Calculations		Experiment	Calculations			Experiment
ν_i	Mode[a]	Harmonic	Anharmonic	Ar	p-H_2	Harmonic	Anharmonic	Ar	Harmonic	Anharmonic	Predicted[b]	p-H_2
ν_1	ν_{OH}	3858 (65)	3677	3650	3651.9 (39)[c]	2809 (40)	2715	2694	3858 (65)	3677	3650	3653.6 (62)[c]
ν_2	a-ν_{CH2}	3289 (8)	3176			2459 (6)	2400		2460 (6)	2396		
ν_3	s-ν_{CH2}	3147 (18)	3082		3038.5 (15)	2275 (19)	2203		2275 (18)	2202	2171	2165.9 (13)
ν_4	$\delta_{s\text{-}CH2}$	1480 (9)	1470	1459	1457.6 (4)	1028 (19)	1013		1031 (16)	1016	1007	1017.1 (24)
ν_5	δ_{OH}	1358 (26)	1315	1334	1332.1 (20)	1055 (27)	1029	1041	1303 (14)	1270	1287	1280.5 (28)
ν_6	ν_{CO}	1224 (112)	1200	1183	1179.2 (112)	1258 (89)	1234	1223	1251 (139)	1221	1200	1212.9 (139)
ν_7	δ_{HCOH}	1051 (47)	1037	1048	1047.0 (63)	763 (24)	756	765	843 (17)	824	832	840.7 (25)
ν_8	τ_{CO}	517 (126)	44			397 (61)	52		428 (128)	248		
ν_9	op-δ	404 (22)	147			302 (21)	195		356 (6)	52		
Reference		This work		40, 41	This work	This work		41	This work			This work

[a]ν: stretch, δ: bend or deformation, δ_S: scissor, τ: torsion, a: antisymmetric, s: symmetric, op: out-of-plane.
[b]Predicted values are derived by multiplying observed wavenumbers of CH_2OH with the calculated isotopic ratio, defined as the ratio of the anharmonic vibrational wavenumber of CD_2OH to that of CH_2OH predicted quantum chemically.
[c]Integrated IR intensities relative to ν_6 of are listed in parentheses.

minimize the error of calculations, we also list the predicted values for CD_2OH in Table III. The predicted values are derived on multiplying the observed wavenumber of CH_2OH with the ratio of calculated anharmonic vibrational wavenumber of CD_2OH to that of natural CH_2OH. Most deviations between observed and predicted vibrational wavenumbers are within 1%. In contrast, predicted vibrational wavenumbers for ν_5 and ν_7 modes of CD_2OD at 1029 and 756 cm^{-1} deviate significantly from observed lines at 1280.5 and 840.7 cm^{-1}. We hence assigned observed lines in group B in experiments with $CD_3OS(O)Cl/p$-H_2 to CD_2OH instead of CD_2OD.

Although lines due to CH_2OH and CD_2OH appeared to be comparable to those of CH_3OSO and CD_3OSO, the estimated mixing ratios of $[CH_3OSO]$:$[CH_2OH]$ and $[CD_3OSO]$:$[CD_2OH]$ are 12−21 and 4−7, respectively, when the observed integrated intensities and predicted IR intensities were used. Similarly, the estimated mixing ratios of $[CH_3OS(O)Cl]_0$:$[CH_2OH]$ (or $[CH_3OH]_0$) and $[CD_3OS(O)Cl]_0$:$[CD_2OH]$ (or $[CD_3OH]_0$) are ∼45 and ∼38, respectively. This also indicates that secondary photolysis or reaction of CH_3OSO and CD_3OSO, but not CH_2OH or CD_2OH, plays an important role in our experiments.

D. Mechanism of formation and diminished cage effect in p-H_2

Lines of *syn*-CH_3OSO appear upon irradiation of the $CH_3OS(O)Cl/p$-H_2 matrix near 239 ± 20 nm. This behavior is consistent with a mechanism according to which, upon photolysis of $CH_3OS(O)Cl$ to form Cl + CH_3OSO, some Cl atoms can escape from the original cage because of the diminished cage effect of p-H_2 so that CH_3OSO becomes isolated without a secondary reaction with the Cl atom. The presence of isolated Cl in p-H_2 is evident from the line at 943.8 cm^{-1}.[42] The diminished matrix cage effect of p-H_2 makes feasible the production of CH_3OSO radicals from photolysis *in situ* of matrix-isolated $CH_3OS(O)Cl$. Although the photolysis of impurity $(CH_3O)_2SO$ at 248 nm yields CH_3 + $CH_3OS(O)O$,[49] we observed no IR absorption line of $CH_3OS(O)O$ in the $CH_3OS(O)Cl/p$-H_2 experiments; this might be due to either $CH_3OS(O)O$ further decomposes or the yield is too small to detect.

The intensity of lines of *syn*-CH_3OSO decreased with further irradiation at the same wavelength because of dissociation of *syn*-CH_3OSO to produce CH_3 and SO_2, shown in Fig. 1(c) as a weak line at 624 cm^{-1} for CH_3 and some lines near 1345 cm^{-1} for SO_2. The SO and SO_2 fragments might react further with Cl atom to produce $ClSO_2$ and ClSO, respectively, as observed in our experiment in small quantities. Another possibility for the production of $ClSO_2$ is that atomic Cl reacts with the SO_2 impurity. The SO_2 fragments might also react with CH_3 to produce CH_3SO_2.

Lines of CH_2OH also appeared upon irradiation of the CH_3OSOCl/p-H_2 matrix; their intensity increased with further irradiation. How CH_2OH was produced in a small proportion is unclear. The reaction of Cl with the CH_3OH impurity might produce CH_2OH. If this reaction is responsible for formation of CH_2OH in experiments of $CH_3OS(O)Cl/p$-H_2, CD_2OH rather than CD_2OD is expected to be produced in experiments of $CD_3OS(O)Cl/p$-H_2 because CD_3OH was employed in the synthesis of $CD_3OS(O)Cl$. In contrast, if photolysis of CH_3OSO would produce CH_2OH + SO, one would expect to observe CD_2OD from photolysis of CD_3OSO, inconsistent with our observation.

V. CONCLUSION

Photo irradiation near 239 nm of a $CH_3OS(O)Cl/p$-H_2 matrix at 3.2 K produced new features at 3028.4 (ν_1), 2999.5 (ν_2), 2950.4 (ν_3), 1465.2 (ν_4), 1452.0 (ν_5), 1417.8 (ν_6), 1165.2 (ν_7), 1152.1 (ν_8), 1147.8 (ν_9), 989.7 (ν_{10}), and 714.5 (ν_{11}) that are assigned to *syn*-CH_3OSO. When a matrix of $CD_3OS(O)Cl/p$-H_2 was used, lines at 2275.9 (ν_1), 2251.9 (ν_2), 2083.3 (ν_3), 1070.3 (ν_4), 1056.0 (ν_5), 1085.5 (ν_6),

1159.7 (ν_7), 920.1 (ν_8), 889.0 (ν_9), 976.9 (ν_{10}), and 688.9 cm^{-1} (ν_{11}) were observed and are assigned to *syn*-CD_3OSO; the mode numbers correspond to those used for *syn*-CH_3OSO. These assignments are based on their photochemical behavior and a comparison of observed and calculated anharmonic vibrational wavenumbers, relative IR intensities, and D-isotopic shifts.

Four bands had been observed for gaseous CH_3OSO.[17] Our results are consistent with the five vibrational modes derived from simulation of rotational contours: 2991, 2956, 1154, 1151, and 994 cm^{-1}. We extended the observation to all 11 vibrational modes within our detection range and characterized the important O−S stretching mode at 714.5 cm^{-1}. The vibrational wavenumbers of CD_3OSO are new.

Weak features observed at 3651.8, 3038.5, 1457.6, 1332.1, 1179.2, and 1047.0 cm^{-1} in $CH_3OS(O)Cl/p\text{-}H_2$ experiments are assigned to CH_2OH. When a matrix of $CD_3OS(O)Cl/p\text{-}H_2$ was used, lines at 3653.6, 2165.9, 1280.5, 1212.9, 1017.1, and 840.7 cm^{-1} were observed and assigned to CD_2OH. CD_2OH might be produced from the reaction of Cl with the impurity CD_3OH that was employed in the synthesis of $CD_3OS(O)Cl$.

The observation of CH_3OSO radical as the major product serves as an example to illustrate that solid $p\text{-}H_2$ has a diminished cage effect, so that isolated CH_3OSO radicals and Cl atoms are produced upon UV photolysis of $CH_3OS(O)Cl$.

ACKNOWLEDGMENTS

We would like to dedicate this paper to Professor Helge Willner on the occasion of his 65th birthday. National Science Council of Taiwan (Grant No. NSC100-2745-M009-001-ASP) and the Ministry of Education, Taiwan ("Aim for the Top University Plan" of National Chiao Tung University) supported this work. The National Center for High-Performance Computing provided computer time. We thank Laurie Butler for sharing their method of synthesis of $CH_3OS(O)Cl$ and their preprint with us.

[1] T. S. Bates, B. K. Lamb, A. Guenther, J. Dignon, and R. E. Stoiber, J. Atmos. Chem. **14**, 315 (1992).
[2] R. J. Charlson, J. E. Lovelock, M. O. Andreae, and S. G. Warren, Nature **326**, 655 (1987).
[3] I. Barnes, K. H. Becker, and N. Mihalopoulos, J. Atmos. Chem. **18**, 267 (1994).
[4] S. B. Barone, A. A. Turnipseed, and A. R. Ravishankara, Faraday Discuss. **100**, 39 (1995).
[5] I. Barnes, J. Hjorth, and N. Mihalopoulos, Chem. Rev. **106**, 940 (2006).
[6] A. J. Frank and F. Turecek, J. Phys. Chem. A **103**, 5348 (1999).
[7] S. R. Davis, J. Phys. Chem. **97**, 7535 (1993).
[8] L. Zhu and J. W. Bozzelli, J. Mol. Struct.: THEOCHEM **728**, 147 (2005).
[9] L. Zhu and J. W. Bozzelli, J. Phys. Chem. A **110**, 6923 (2006).
[10] B. J. Ratliff, X. Tang, L. J. Butler, D. E. Szpunar, and K.-C. Lau, J. Chem. Phys. **131**, 044304 (2009).
[11] B. W. Alligood, B. L. FitzPatrick, E. J. Glassman, L. J. Butler, and K.-C. Lau, J. Chem. Phys. **131**, 044305 (2009).
[12] X. Li, L. Meng, Y. Zeng, and S. Zheng, Chin. J. Chem. **28**, 896 (2010).
[13] S. E. Wheeler and H. F. Schaefer III, J. Phys. Chem. A **113**, 6779 (2009).
[14] L.-K. Chu and Y.-P. Lee, J. Chem. Phys. **133**, 184303 (2010).
[15] B. C. Gilbert, C. M. Kirk, R. O. C. Norman, and H. A. H. Laue, J. Chem. Soc., Perkin Trans. II (4), 497 (1977).
[16] C. Chatgilialoglu, B. C. Gilbert, C. M. Kirk, and R. O. C. Norman, J. Chem. Soc., Perkin Trans. II (8), 1084 (1979).
[17] J.-D. Chen and Y.-P. Lee, J. Chem. Phys. **134**, 094304 (2011).
[18] Y.-P. Lee, J. Chin. Chem. Soc. **39**, 503 (1992).
[19] Y.-P. Lee, J. Chin. Chem. Soc. **52**, 641 (2005).
[20] M. Bahou, C.-W. Huang, Y.-L. Huang, J. Glatthaar, and Y.-P. Lee, J. Chin. Chem. Soc. **57**, 771 (2010).
[21] T. Momose, M. Miki, M. Uchida, T. Shimizu, I. Yoshizawa, and T. Shida, J. Chem. Phys. **103**, 1400 (1995).
[22] N. Sogoshi, T. Wakabayashi, T. Momose, and T. Shida, J. Phys. Chem. A **101**, 522 (1997).
[23] M. Fushitani, N. Sogoshi, T. Wakabayashi, T. Momose, and T. Shida, J. Chem. Phys. **109**, 6346 (1998).
[24] M. Bahou and Y.-P. Lee, J. Chem. Phys. **133**, 164316 (2010).
[25] C.-W. Huang, Y.-C. Lee, and Y.-P. Lee, J. Chem. Phys. **132**, 164303 (2010).
[26] J. C. Amicangelo and Y.-P. Lee, J. Phys. Chem. Lett. **1**, 2956 (2010).
[27] Y.-F. Lee and Y.-P. Lee, J. Chem. Phys. **134**, 124314 (2011).
[28] B. Golec and Y.-P. Lee, J. Chem. Phys. **135**, 174302 (2011).
[29] J. C. Amicangelo, B. Golec, M. Bahou, and Y.-P. Lee, Phys. Chem. Chem. Phys. **14**, 1014, (2012).
[30] L.-K. Chu and Y.-P. Lee, J. Chem. Phys. **124**, 244301 (2006).
[31] Y.-P. Lee, Y.-J. Wu, R. M. Lees, L.-H. Xu, and J. T. Hougen, Science **311**, 365 (2006).
[32] P. L. Raston and D. T. Anderson, Phys. Chem. Chem. Phys. **8**, 3124 (2006).
[33] G. Berti, J. Am. Chem. Soc. **76**, 1213 (1954).
[34] M. J. Frisch, G. W. Trucks, H. B. Schlegel *et al.*, GAUSSIAN 09, Revision A.02, Gaussian, Inc., Wallingford, CT, 2009.
[35] T. H. Dunning, Jr., J. Chem. Phys. **90**, 1007 (1989).
[36] D. E. Woon and T. H. Dunning, Jr., J. Chem. Phys. **98**, 1358 (1993).
[37] A. Borba, A. Gómez-Zavaglia, P. N. N. L. Simões, and R. Fausto, J. Phys. Chem. A **109**, 3578 (2005).
[38] D. T. Anderson, R. J. Hinde, S. Tam, and M. E. Fajardo, J. Chem. Phys. **116**, 594 (2002).
[39] T. Shimanouchi, "Tables of molecular vibrational frequencies consolidated volume II," J. Phys. Chem. Ref. Data **6**, 993 (1972).
[40] M. E. Jacox and D. E. Milligan, J. Mol. Spectrosc. **47**, 148 (1973).
[41] M. E. Jacox, Chem. Phys. **59**, 213 (1981).
[42] P. L. Raston and D. T. Anderson, J. Chem. Phys. **126**, 021106 (2007).
[43] A. G. Hopkins and C. W. Brown, J. Chem. Phys. **62**, 2511 (1975).
[44] M. Bahou, S.-F. Chen, and Y.-P. Lee, J. Phys. Chem. A **104**, 3613 (2000).
[45] L.-K. Chu, Y.-P. Lee, and E. Y. Jiang, J. Chem. Phys. **120**, 3179 (2004).
[46] T. Shimanouchi, "Tables of molecular vibrational frequencies consolidated volume I," National Bureau of Standards, 1 (1972).
[47] M. E. Jacox, J. Mol. Spectrosc. **66**, 272 (1977).
[48] A. Snelson, J. Phys. Chem. **74**, 537 (1970).
[49] B. W. Alligood, C. C. Womack, D. B. Straus, F. R. Blasé, and L. J. Butler, J. Chem. Phys. **134**, 194304 (2011).
[50] J. Rufus, G. Stark, P. L. Smith, J. C. Pickering, and A. P. Thorne, J. Geophys. Res. **108**, 5011, doi:10.1029/2002JE001931 (2003).
[51] S. O. Danielache, C. Eskebjerg, M. S. Johnson, Y. Ueno, and N. Yoshida, J. Geophys. Res. **113**, D17314, doi:10.1029/2007JD009695 (2008).
[52] C. S. Effenhauser, P. Felder, and J. R. Huber, Chem. Phys. **142**, 311 (1990).